Available online at www.sciencedirect.com
ScienceDirect
Trans. Nonferrous Met. Soc. China 31(2021) 1628−1640
Transactions of Nonferrous Metals Society of China
www.tnmsc.cn

Static coarsening behavior of equiaxed α phase in Ti−8Al−1Mo−1V alloy

Xiao-hui SHI[1,2], Zu-han CAO[1], Zhi-yuan FAN[1], Jürgen ECKERT[2,3], Jun-wei QIAO[1]

1. College of Materials Science and Engineering, Taiyuan University of Technology, Taiyuan 030024, China;
2. Erich Schmid Institute of Materials Science, Austrian Academy of Sciences, LeobenA-8700, Austria;
3. Department of Materials Science, Chair of Materials Physics, Montanuniversität Leoben, LeobenA-8700, Austria

Received 15 July 2020; accepted 25 January 2021

Abstract: To get a deep understanding of the evolution behavior of equiaxed α phase in Ti−8Al−1Mo−1V alloy during annealing, its static coarsening mechanism was studied based on the calculations of coarsening exponent n and the activation energy for α boundary migration. The result of n=6 indicates a special coarsening mechanism of equiaxed α phase. The activation energy for α boundary migration is calculated to be 138 kJ/mol, which is close to the activation energy for grain growth of pure α-Ti. It is revealed that the coarsening of equiaxed α can be mainly attributed to the self-diffusion of Ti atoms across the α/α boundaries. Based on the experimental findings, a static coarsening kinetics model of equiaxed α grains in the α+β field is established. At last, the effects of the coarsening behavior of equiaxed α on tensile properties were studied.

Key words: static coarsening; kinetics; model; tensile properties; Ti−8Al−1Mo−1V

1 Introduction

Titanium (Ti) alloys are widely used in aerospace fields due to their high specific strength, low density and good corrosion resistance [1]. α (hexagonal close packing structure) and β (body-centered cubic structure) are the two typical phases in Ti alloys, and their relative contents can vary a lot in different Ti alloy systems or under different treatments. For Ti alloy billets subjected to different treatments, the α phase in the microstructure can exhibit two different morphologies and different mechanical behaviors. Generally speaking, lamellar α is retained after direct cooling from the β phase field, and it is favorable for improving the fracture toughness and the fatigue crack propagation resistance of Ti alloys [2]. In contrast, equiaxed α, which is formed through deformation and subsequent static annealing of lamellar α, can elevate the plasticity and the fatigue crack initiation resistance [3]. In most applications, a certain amount of equiaxed α is introduced in the microstructure to ensure good overall mechanical properties of components. Nowadays, with the much stricter request of improved mechanical performance of Ti alloys, a more accurate control of the volume fraction and morphology of equiaxed α in the microstructure becomes essential.

The volume fraction of equiaxed α is strongly affected by the deformation parameters, which has been extensively studied [4−6]. The final size and morphology of equiaxed α can be mostly tuned during subsequent static annealing. However, detailed research on how the size and morphology of equiaxed α can be tuned appropriately is still insufficient. The evolution process of a phase during annealing is typically named "static coarsening" [7], which was initially explained by the well-known Lifshitz−Slyosov−Wagner (LSW) theory [8]. A severe limitation of the LSW theory is that it only holds true for systems comprising

Corresponding author: Xiao-hui SHI, Tel: +86-351-6010533, E-mail: sxhtough@126.com
DOI: 10.1016/S1003-6326(21)65603-0

terminal solid solutions and a very infinitesimal volume fraction of the target phase [9]. For titanium alloys, none of the phases is a terminal solid solution. Furthermore, the volume fraction of equiaxed α in the microstructure is generally nonnegligible. Therefore, the LSW theory is not applicable any more. Some important researches regarding the static coarsening behavior of equiaxed α with limited volume fraction (less than 50 vol.%) have been conducted [10−12]. SEMIATIN et al [10,11] studied the static coarsening behavior of Ti−6Al−2Sn−4Zr−2Mo−0.1Si and Ti−6Al−4V alloys with ultrafine, equiaxed α microstructure. They found that the static coarsening processes of the equiaxed α for these two alloys are controlled by bulk diffusion and follow modified LSW kinetics (i.e., using a modification considering the volume fraction effect and the fact that the phases are not terminal solid solutions) [13]. SARGENT et al [12] studied the static coarsening response of the Ti−6Al−4V alloy via a series of heat treatments. They found that at all test temperatures, static coarsening of α particles occurs by diffusion- controlled kinetics (that can be interpreted using the modified LSW theory). The above-mentioned researches prove that the static coarsening behavior of equiaxed α with limited volume fraction (less than 50 vol.%) can be described by the modified LSW model. On the other hand, it is well agreed that different volume fractions of the target phase in the microstructure may lead to intrinsically different coarsening behavior.

The Ti−8Al−1Mo−1V (Ti811, for short) alloy is a near α titanium alloy which is known for its low density, high microstructure stability and good damping capacity [14]. Therefore, it is widely used in manufacturing critical components of aircrafts, such as turbine blades. Due to the high content of α stabilizing elements (namely Al), Ti811 alloy always contains a high volume fraction of equiaxed α. Hence, the size and morphology of equiaxed α may exert strong influence on the mechanical response of the material. In the present work, the Ti811 alloy with a high initial volume fraction of equiaxed α was selected for systematically investigating the coarsening behavior of equiaxed α during static annealing and its correlation with the tensile properties.

2 Experimental

The as-received Ti811 alloy was a hot-rolled bar with a diameter of 45 mm. Its chemical compositions were Al 8.1, Mo 1.05, V 0.99 (wt.%), with less than 0.15 wt.% of impurity elements (C, N, O and Fe), and Ti as balance. The β transus temperature was determined to be 1035 °C. Figures 1(a, b) show the initial microstructure morphologies in different magnifications. Equiaxed α particles with an average grain around 5 μm are homogeneously distributed throughout the material. Some primary α lamellae were not thoroughly fragmented during hot rolling, and can still be observed in the microstructure.

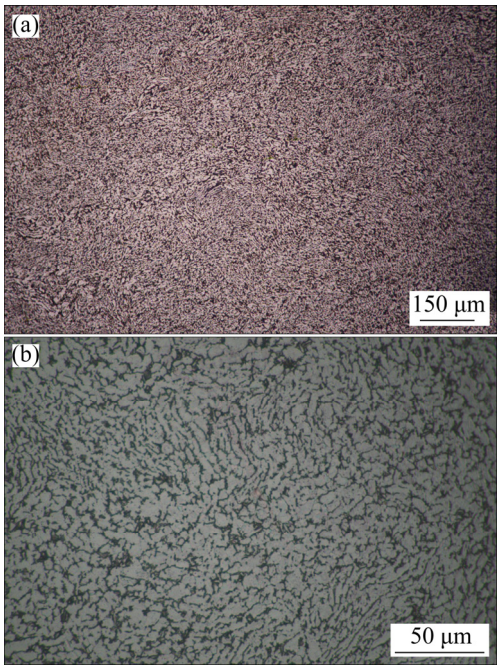

Fig. 1 Initial microstructure morphologies of as-received Ti811 alloy: (a) In low magnification; (b) In high magnification

The samples with dimensions of ϕ45 mm × 10 mm were sectioned from the billet and then subjected to static annealing treatments for 1, 2, 3, 5, 6 and 8 h, respectively, at 910 °C followed by air cooling (AC). Metallographic specimens for all treatments were prepared through wire-electrode cutting. After grinding, polishing, and etching using a solution of V(HF):V(HNO_3):V(H_2O)=1:3:13, metallographic images were captured using a Leica 6000M OM (optical microscope). The average size of the equiaxed α grains after each treatment was

calculated using line intersection method. Measuring the total number of segments intersecting equiaxed α grains, N, and correlating it with the total length of the segments, l, allow to calculate the average size of equiaxed α grains, D, by dividing l by N. To ensure accurate results, at least 100 equiaxed α grains for each treatment were sampled. According to the stereology theory [15], the volume fraction of equiaxed α is equivalent to their area fraction in the microstructure, which was quantitatively analyzed by means of the image processing software Image Pro Plus 6.0 (IPP 6.0).

To ensure the reproducibility of the results, chemical composition measurements of equiaxed α and transformed β were carried out using Hitachi SU8010 and JSM-IT200 SEM (scanning electron microscope). EBSD (electron back-scattered diffraction) analysis was conducted using the HKL-EBSD system attached to a Hitachi S−3400 N SEM. The EBSD specimen preparation is a surface-sensitive technique. To get valuable EBSD data, mounting, grinding and polishing were conducted successively to pursue the minimum surface topography. The scanning step was set to be 600 nm during characterization. Two specimens for each treatment were chosen for tensile tests using an Instron 5969 mechanical testing machine at a constant strain rate of 2×10^{-3} s^{-1}. The fracture surface morphologies of the fractured tensile specimens were observed by SEM.

3 Results and discussion

3.1 Evolution behavior of equiaxed α

Figures 2(a−f) show the microstructure features after different static annealing treatments. Apparently, the annealing time has noticeable influence on the size, volume fraction as well as the morphology of equiaxed α.

As the research emphasis of this work, the size evolution of equiaxed α is analyzed firstly. Figure 2(a) shows the microstructure features of the Ti811

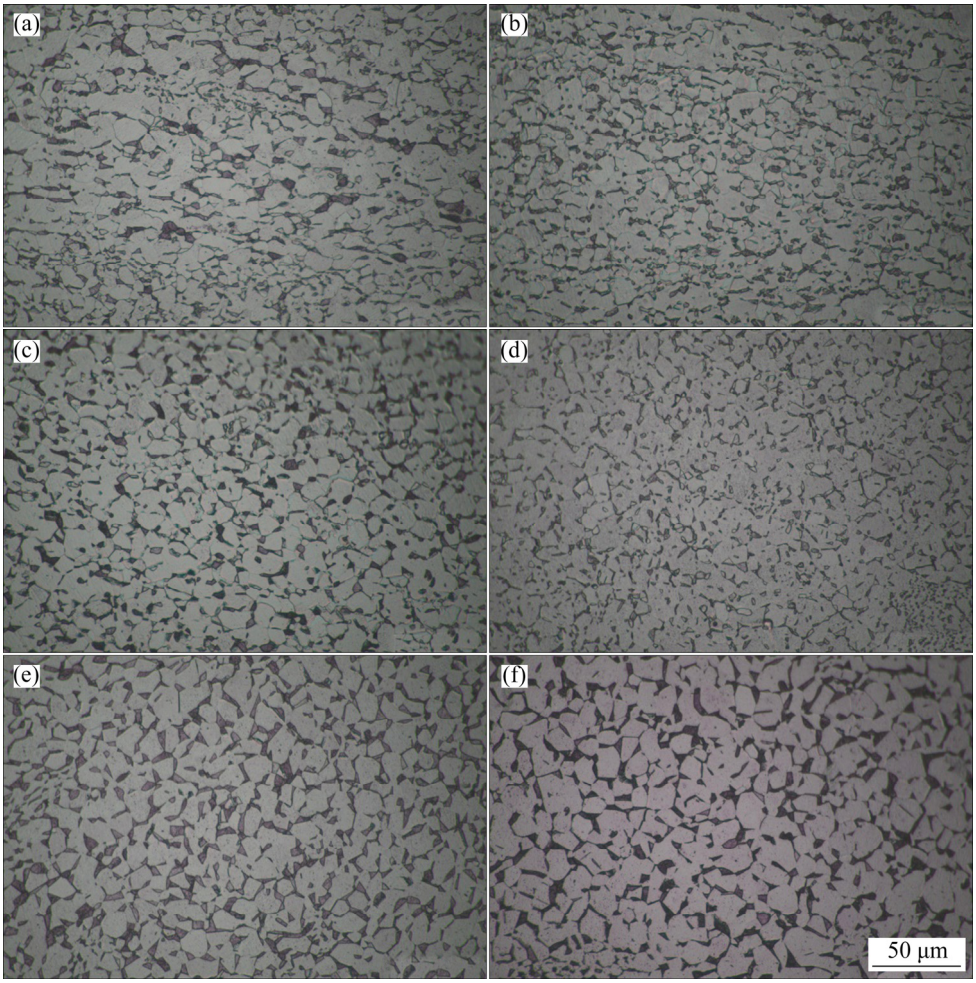

Fig. 2 Microstructure features after annealing at 910 °C for different time: (a) 1 h; (b) 2 h; (c) 3 h; (d) 5 h; (e) 6 h; (f) 8 h

alloy after annealing for 1 h. Obvious coarsening of equiaxed α can be found by comparing with the initial microstructure. However, a high level of nonuniformity of the size of the equiaxed α grains can be observed. This indicates that the coarsening is not stable during the first 1 h of annealing, but due to the high density of retained dislocations in the microstructure after hot rolling, static globularization occurs simultaneously. By increasing the annealing time to 2 h or longer, a homogeneous equiaxed α size can be realized. This indicates that stable coarsening begins to occur after annealing for 2 h. For this reason, the annealing time of 2 h was taken as the initial state for studying the static coarsening mechanisms and kinetics.

Equiaxed α shows continuous coarsening with increasing annealing time (>2 h), which is driven by a reduction of the interfacial energy [16]. The variation of measured average α grain size D for different annealing time is shown in Fig. 3(a), revealing that D follows a parabolic growth trend with increasing annealing time. The longer the annealing time is, the slower the coarsening rate will be. After annealing for 8 h, D reaches 9.83 μm.

The volume fractions of equiaxed α (f_α) for different annealing time were also measured, as shown in Fig. 3(b). It can be found that f_α increases firstly and then slowly decreases with increasing annealing time. When the annealing time is below 3 h, f_α remains around 75%. This is mainly due to the fact that static recrystallization plays an important role in such short periods, during which the β-to-α transformation is not apparent. When the annealing time increases to 5 h, f_α exhibits a slight increase, reaching 81.6%. The coarsening of equiaxed α during this period is partially attributed to the β-to-α transformation. When the annealing time increases beyond 5 h, f_α slowly decreases again. After annealing for 8 h, f_α drops down to around 75%. It is supposed that the coarsening of equiaxed α in this stage is merely attributed to the incorporation of small α grains into adjacent big α grains. At the same time, some small α grains may dissolve again in the β phase.

Figures 4(a−c), 4(d−f) and 4(g−i) show SEM micrographs and the corresponding Al and Mo distribution maps for annealing time of 2, 5 and 8 h, respectively. Table 1 lists the semi-qualitative results (in wt.%) of the Al and Mo contents characterized by EDS (energy-dispersive X-ray spectroscopy). Comparing Figs. 4(b), (e) and (h) reveals that the Al content in the β zone after 5 h of annealing is lower than that after 2 h and 8 h of annealing. The semi-quantitative results (it should be noted that the values only have contrast significance) shown in Table 1 also prove this results. The Mo content in the β zone, however, reaches a peak value after annealing for 5 h. This indicates that the β-to-α transformation occurs for annealing time below 5 h, during which Al from the β phase diffuses to the newly-formed α phase, and the redundant Mo in the newly-formed α phase diffuses to the retained β phase. Once the annealing time is above 5 h, a reverse transformation from α to β occurs, and the diffusion direction of Al and Mo is also reversed. Based on the above discussion, it is understandable that the Al and Mo contents along the scanning line in the SEM graph show higher fluctuation amplitudes after 5 h of annealing than after 8 h, as depicted in Fig. 5.

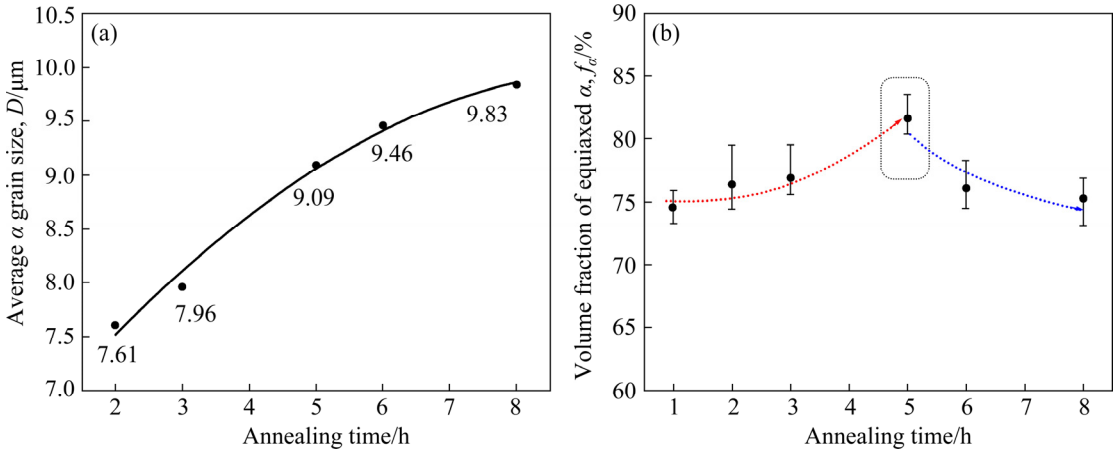

Fig. 3 Quantitative results of evolution of equiaxed α after different annealing time: (a) Average α grain size; (b) Volume fraction of equiaxed α

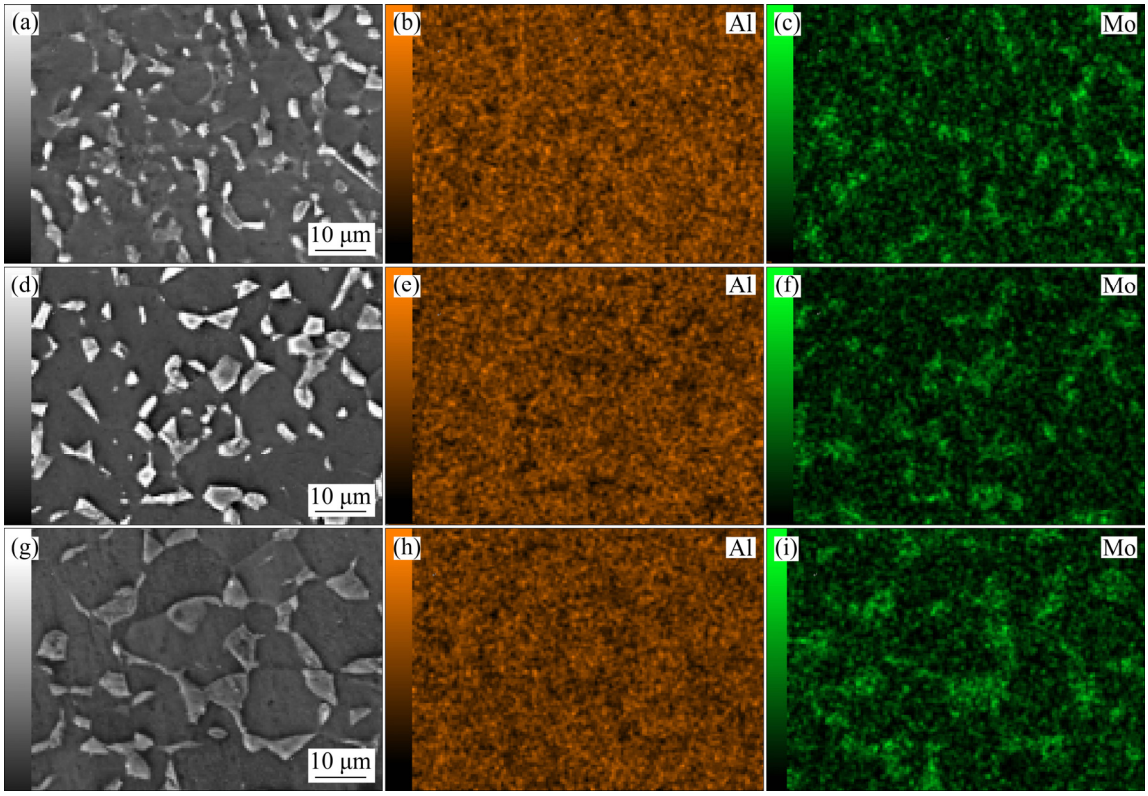

Fig. 4 SEM micrographs and corresponding Al and Mo distribution maps for Ti811 alloy after static annealing for different time: (a−c) 2 h; (d−f) 5 h; (g−i) 8 h

Table 1 Semi-qualitative results (wt.%) of chemical compositions characterized by EDS after annealing

Element	As-received		910 °C, 2 h		910 °C, 5 h		910 °C, 8 h	
	α	β	α	β	α	β	α	β
Al	−	−	6.95	6.95	7.19	5.63	7.72	6.29
Mo	−	2.50	−	2.13	−	3.37	−	3.01

Some interesting phenomena can be observed regarding the morphology evolution of equiaxed α. Figure 6 shows the morphologies of equiaxed α after annealing for different time. Taking the annealing time of 5 h as demarcation point, it can be clearly observed that the morphology of the equiaxed α grains shows two changing stages. When the annealing time is below 5 h, the morphology of the α grains changes from a short rod-like shape at the initial state (see Fig. 6(a)) to a near-spherical shape with increasing annealing time, as shown in Figs. 6(b, c), as it is typical for a static spheroidization process. However, when the annealing time increases beyond 5 h, the morphology of the equiaxed α grains changes towards polygonization. Namely, the original curved α/α and α/β boundaries gradually become straight, as shown in Figs. 6(d−f). This is a natural result of grain coarsening. As mentioned above, the driving force of grain coarsening is essentially the reduction in interfacial energy of the grain boundaries (namely the reduction in the total grain boundary area). To this end, the thermodynamic system impels the boundaries to migrate towards their respective centers of curvature [17]. As a result, the grain boundary curvature decreases with increasing annealing time. Accordingly, the grain boundaries become more and more straight. Based on the work of MASON [18], and PATTERSON and LIU [19], the grain coarsening rate is proportional to the grain boundary curvature. This leads to a lower coarsening rate with increasing annealing time, which is in accordance with the results shown in Fig. 3(a). Once the grain boundary curvature approaches zero, grain coarsening finally ceases.

To get more detailed insights into the microstructure morphology undergone static coarsening, EBSD analyses were conducted. Figure 7 shows the EBSD characterization results of the microstructure after annealing for 8 h. Figures 7(a, b) reveal that

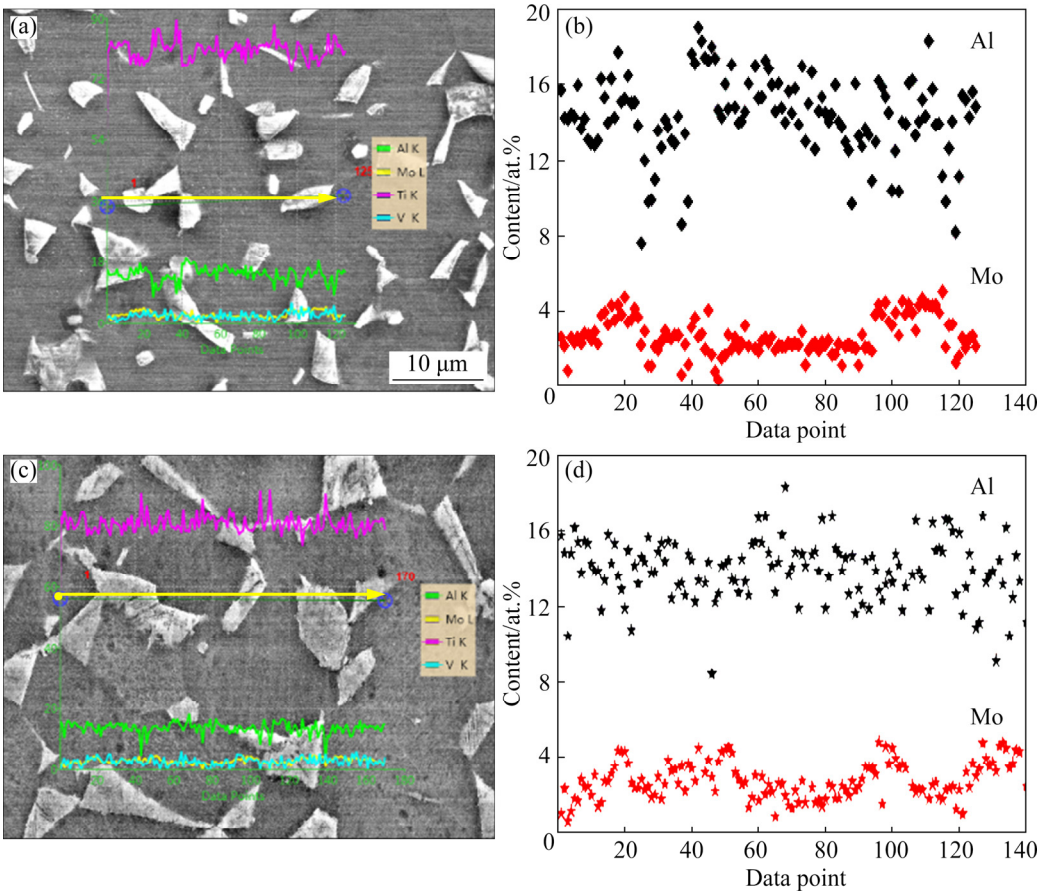

Fig. 5 Line scans and corresponding Al and Mo content fluctuations along lines: (a, b) 5 h; (c, d) 8 h

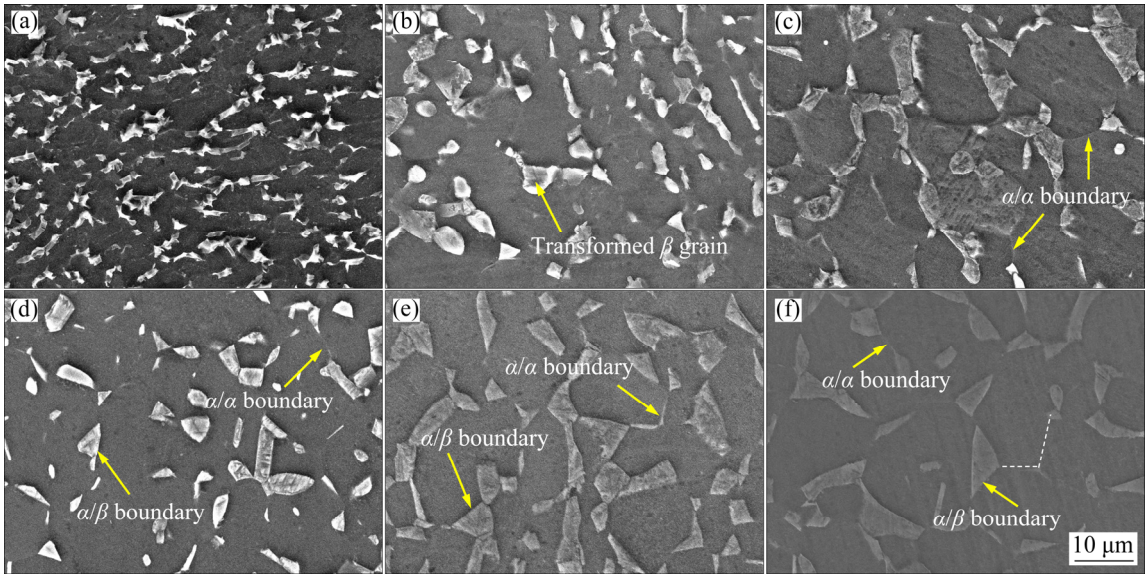

Fig. 6 Morphologies of equiaxed α after annealing for different time: (a) Ar-received; (b) 2 h; (c) 3 h; (d) 5 h; (e) 6 h; (f) 8 h

most of the transformed β grains are individually dispersed on the boundaries of equiaxed α grains. The misorientation angle distribution map of adjacent grains (see Fig. 7(c)) verifies that the α/α boundaries are mainly high-angle boundaries. However, due to the lack of precipitations on them, the α/α boundaries are not obvious when characterized by OM and SEM.

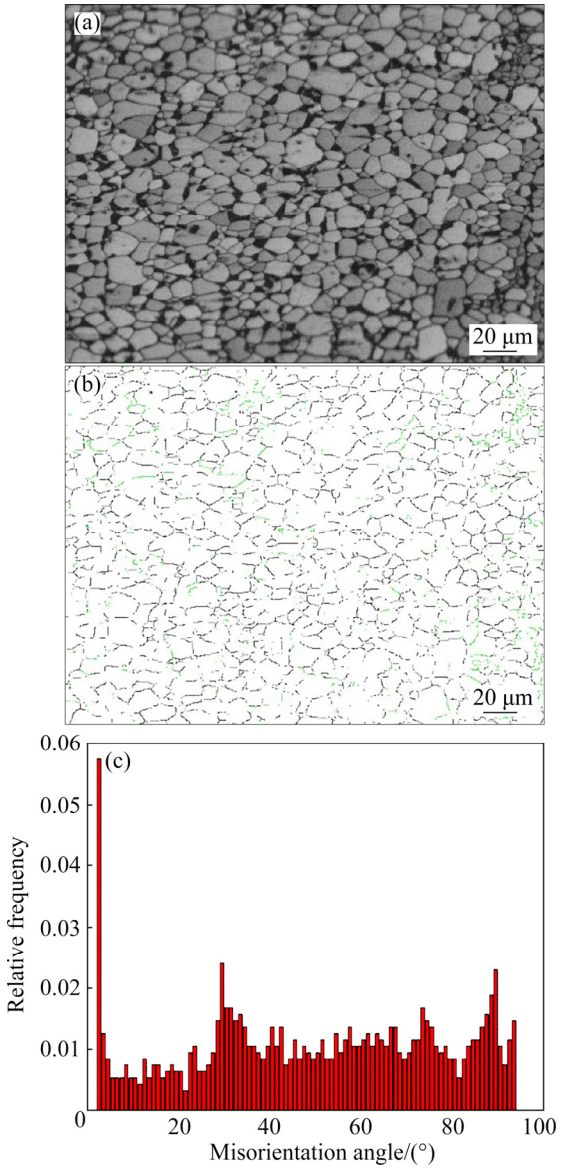

Fig. 7 EBSD characterization results of microstructure after annealing for 8 h: (a) Diffraction contrast map; (b) Grain boundary map; (c) Misorientation angle distribution map of adjacent grains

3.2 Static coarsening mechanism and kinetics

It is widely accepted that the generalized expression for grain coarsening can be written in the following form [16]:

$$D^n - D_0^n = k(t - t_0) \quad (1)$$

where t and D are the annealing time and the corresponding average grain size, and t_0 and D_0 are the initial time and the initial average grain size, respectively. k is the rate constant, which depends on the chemical compositions and the temperature, but not on grain size [20]. The exponent n is usually larger than 2 [21].

According to MARTIN et al [13], the value of n precisely reflects the actual coarsening mechanism. When n is equal to 2, 3, 4 and 5, the atom transfer through the second phase/matrix interface, through the lattice diffusion (described by LSW or modified LSW model), through the grain boundaries and through the low angle boundaries (namely dislocation) are the coarsening rate controlling process, respectively. In the present work, the n value should be firstly determined.

According to Eq. (1), the n value must meet the condition under which the scope of $(D^n - D_0^n)$ vs $(t-t_0)$ curve is a constant (namely k). By plotting $(D^n - D_0^n)$ vs $(t-t_0)$ curves for different n values, the correct n can be screened out once the linear correspondence between $(D^n - D_0^n)$ and $(t-t_0)$ is realized. Before that, t_0 and D_0 should be determined. As described above, a homogeneous equiaxed α grain size can only be realized for annealing time above 2 h. Thus t_0 is taken as 2 h, and the corresponding D_0 is 7.61 μm. Figure 8 shows the plots of $(D^n - D_0^n)$ vs $(t-t_0)$ (t>2 h) for different n values (2, 3, 4, 5, 6, 8). It can be clearly observed that the best linear correspondence between $(D^n - D_0^n)$ and $(t-t_0)$ can be realized when n equals 6 (see Fig. 8(e)), for which the adjusted R^2 is 0.993. It should be noted that n=6 does not correspond to any coarsening mechanism described above. Therefore, the LSW model (including the modified LSW model) and the other models (for example, WAGNER model, KIRCHNER model, and ARDELL model) presented in Ref. [13] are not applicable for describing the coarsening behavior of equiaxed α grains in the present work. This can be explained from the following aspects. Firstly, the premise of the LSW model is that the spacing between the precipitates must be much larger than their mean radius. This requires a very small volume fraction of particles. However, the f_a values studied in the present work are generally above 75%. Thus, the lattice diffusion mechanism (n=3) is inapplicable. Secondly, the limited α/β and β/β boundary area renders the interface interaction mechanism (n=2) and grain boundary mechanism (n=4) invalid, respectively. Thirdly, at the annealing temperature of 910 °C, a nearly fully recrystallized microstructure can be obtained after annealing 2 h or longer. In this situation, the dislocation density is very small, and the coarsening of equiaxed α through low angle boundaries (n=5) is unrealistic.

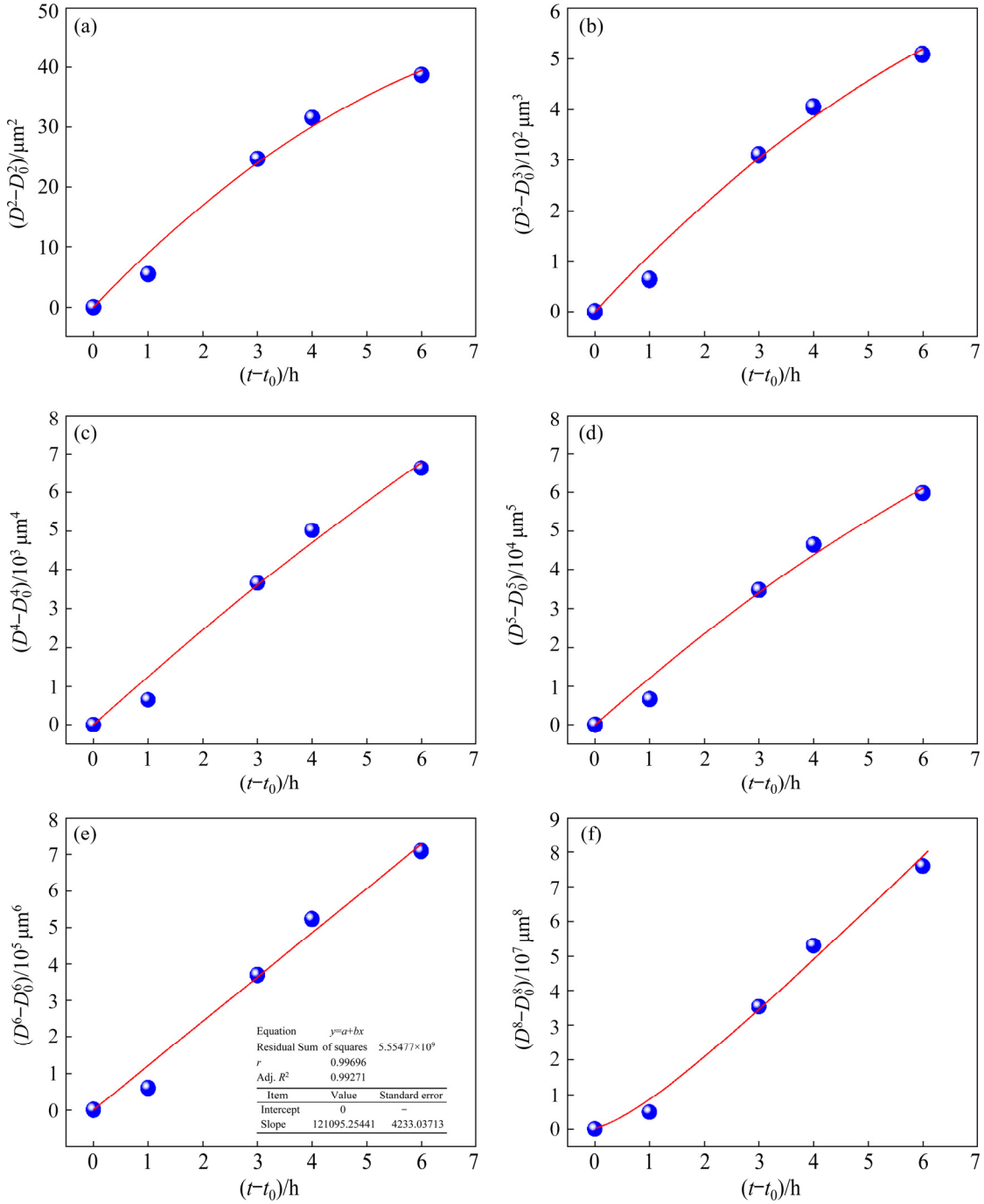

Fig. 8 Plots of ($D^n - D_0^n$) vs ($t-t_0$) for n values of 2 (a), 3 (b), 4 (c), 5 (d), 6 (e) and 8 (f)

Several researchers have conducted pioneering studies [16,22,23] on the coarsening behavior of equiaxed α with high f_α (≥50%). JOHNSON et al [22] investigated the grain growth behavior of a microduplex Ti−6Al−4V alloy with nearly equal phase ratios. The exponent n was calculated to be 5. This indicated a dislocation diffusion mechanism, as described above. However, this mechanism was discounted based on the calculation of diffusivity. Finally, it was suggested that the regulating coarsening mechanism is the diffusion of vanadium along α/α boundaries. GREWAL and ANKEM [23] investigated isothermal particle growth for several Ti−Mn and Ti−V alloys containing varying amounts of α phase at 700 °C. They found that diffusion processes predominately occurred in the α phase when the volume fraction of β phase was small, which was consistent with the findings by JOHNSON et al [22].

According to these investigations, it can be

concluded that the coarsening of equiaxed α in the present work can be mainly attributed to the diffusion of atoms across the α/α boundaries. This leads to the migration of α boundaries. Consequently, favorable α grains grow at the expense of adjacent unfavorable grains. This is similar to the grain coarsening behavior of pure metals or single-phase alloys [24−26]. However, there is around 20−25 vol.% of β in microstructure. Therefore, it cannot be neglected that equiaxed α grain coarsening may to some extent be attributed to the β-to-α transformation for annealing time below 5 h. A schematic illustration of the possible coarsening process of equiaxed α grains is depicted in Fig. 9.

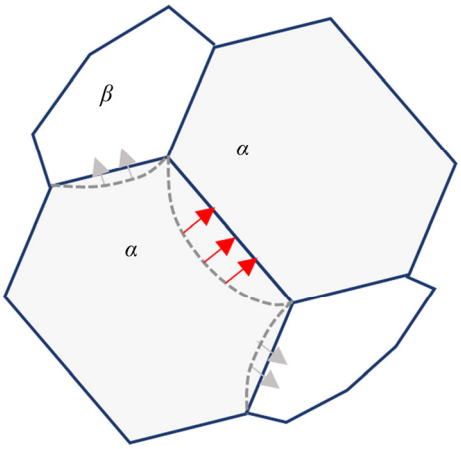

Fig. 9 Schematic illustration of possible coarsening process of equiaxed α grains

Elucidating the diffusion mode which plays the decisive role in the α boundary migration process is another important issue to be solved. This could be related to self-diffusion of Ti atoms or the diffusion of (Al, Mo, V) solute atoms. Hence, it is essential to analyze the static coarsening kinetics of equiaxed α grains. According to Fig. 8(e), the calculated exponent n and the rate constant k in Eq. (1) equal 6 and 1.21×10^5 μm^6/h, respectively. An exclusively theoretical k model exists for a specific n value [13]. However, the k model corresponding to n=6 was not proposed before. As described above, the α boundary migration dominates the coarsening process in the present work. Thus, Eq. (2) [27], which is the typical formula for describing the rate constant of the boundary migration process, may be applicable:

$$k=k_0\exp[-Q_g/(RT)] \quad (2)$$

where k_0 is a material constant, and R is the universal gas constant, which is equal to 8.314 J/(mol·K). T is the thermodynamic temperature, which is 1183 K (910 °C) in the present work. Q_g is the activation energy for boundary migration. According to JOHNSON et al [22], the activation energy Q_g is correlated to a particular diffusion mechanism. To get the Q_g value in the present work, k_0 should be firstly determined.

In 1957, FELTHAM [28] established a theoretical model to calculate k_0:

$$k_0=8Vl\sigma/h \quad (3)$$

where V is the volume per atom, σ is the specific surface energy, l is the lattice spacing and h is the Planck's constant, which is 6.63×10^{-34} J·s [29]. The atomic radius of Ti is 0.145 nm [30], and its volume is 1.28×10^{-11} μm^3. The lattice constant of Ti is 0.295 nm along the a axis, and 0.468 nm along the c axis [31]. l adopts an average value of 3.82×10^{-4} μm. ROTH and SUPPAYAK [32] measured the grain boundary free energy of pure titanium at different temperatures. Based on their data, the specific surface energy σ of α/α boundary can be regarded as 0.7 J/m^2. By substituting the above parameters into Eq. (3), the k_0 value was calculated to be 1.49×10^{11} μm^2/h. By substituting the k_0 value into Eq. (2), the activation energy for α boundary migration in the present work, namely Q_g, equals 138 kJ/mol.

Based on work by GIL and PLANELL [20], the activation energy for grain growth of pure α-Ti is about 100 kJ/mol. WU et al [16] studied Ti−Al−Zr−Mo−V alloy and found that the diffusion rate of Mo is the slowest and becomes the rate-controlling solute. Based on the research by XU et al [33], the diffusion activation energy of Mo (1 at.%) in dilute α-Ti is about 2.4 eV, namely 231 kJ/mol. Apparently, the Q_g value in the present work is much closer to the activation energy for grain growth of pure α-Ti. This indicates that the coarsening of equiaxed α is mainly due to the self-diffusion of Ti atoms. It should also be noted that the Q_g value is slightly higher than the activation energy for grain growth of pure α-Ti. This is due to the solute drag effect of the solute elements, i.e., Al, Mo and V.

Consequently, for the special situation in the present work, the static coarsening kinetics model of equiaxed α grains can be described as

$$D^6 - 7.61^6 = 1.49\times10^{11}\exp\left(\frac{-138000}{1183R}\right)(t-2) \quad (4)$$

where t>2 h, and D is the average grain size in the unit of μm.

In a broader sense, Eq. (5) can be applied to describing the static coarsening kinetics of equiaxed α grains for Ti811 alloy in the α+β field, under the condition that f_α is obviously larger than 50%. D_0, t_0 and n at a given annealing temperature should be recalculated:

$$D^n - D_0^n = 1.49\times10^{11}\exp\left(\frac{-138000}{RT}\right)(t-t_0) \quad (5)$$

3.3 Tensile properties

The static coarsening behavior of equiaxed α grains may exert an obvious influence on the mechanical properties of the Ti811 alloy. Figure 10 shows a comparison of the tensile curves and the tensile properties for samples subjected to annealing for different time. Table 2 lists their specific tensile data. The strength values exhibit small fluctuations (30−40 MPa) and generally become stable after annealing for 3 h or longer. The explanation for this behavior is as follows. It is well known that the volume fraction of precipitated secondary α within the retained β influences the strengthening of titanium alloys. However, the small volume fraction of retained β in the present work leaves little space for strength adjustment. Once the dislocations retained in the as-received alloy are eliminated during annealing and all microstructure features become stable, the strength also becomes stable.

Interestingly, the static coarsening behavior of equiaxed α shows a distinct influence on the plasticity of the Ti811 alloy. Generally speaking, the elongation shows a two-step increase with increasing annealing time, as shown in Fig. 10(b). The as-received alloy has the lowest elongation of 12.8%. Then, it increases to near 17% and remains almost stable for annealing time of 1−3 h. The large increase in elongation is mainly due to static recrystallization. By increasing the annealing time to 5 and 6 h, the elongation increases to the around 19%. This is due to coarsening of the equiaxed α grains which reduces the interfacial blocking effect on dislocation movements. For 8 h of annealing, continuous coarsening of equiaxed α grains and polygonization of α grain boundaries improve the dislocation mobility further. The elongation at this stage reaches the highest value of 21.1%. It is supposed that the plasticity of the Ti811 alloy reaches a stable value upon increasing the annealing time to a critical value, due to the fact that all the

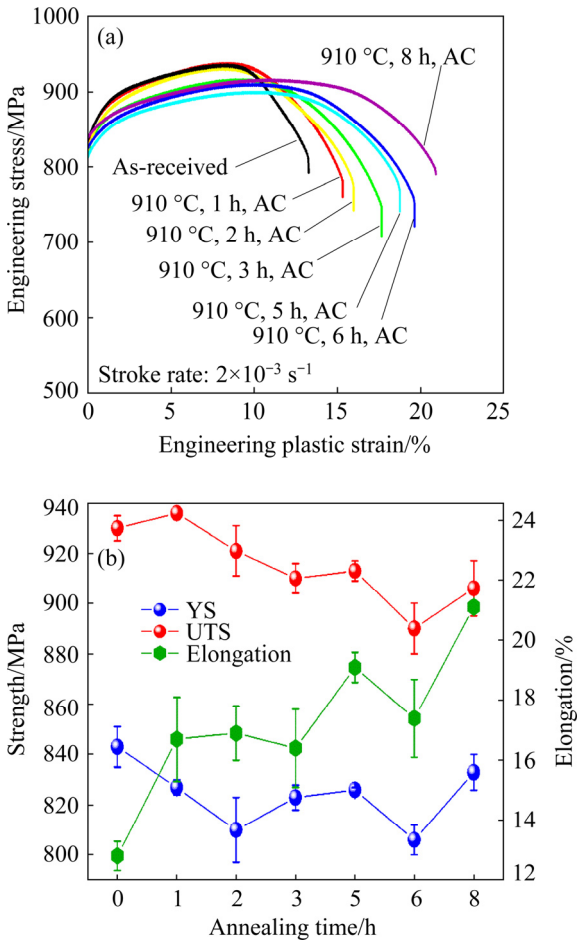

Fig. 10 Comparison of tensile curves and tensile properties for Ti811 samples subjected to annealing for different time: (a) Tensile curves; (b) Tensile properties

Table 2 Tensile property values of Ti811 alloy after annealing for different time

Heat treatment	YS/ MPa	UTS/ MPa	Elongation/ %
As-received	843±8	930±5	12.8±0.5
910 °C, 1 h, AC	827±3	936±1	16.7±1.4
910 °C, 2 h, AC	810±13	921±10	16.9±0.9
910 °C, 3 h, AC	823±5	910±6	16.4±1.3
910 °C, 5 h, AC	826±1	913±4	19.1±0.5
910 °C, 6 h, AC	806±6	890±10	17.4±1.3
910 °C, 8 h, AC	833±7	906±11	21.1±0.1

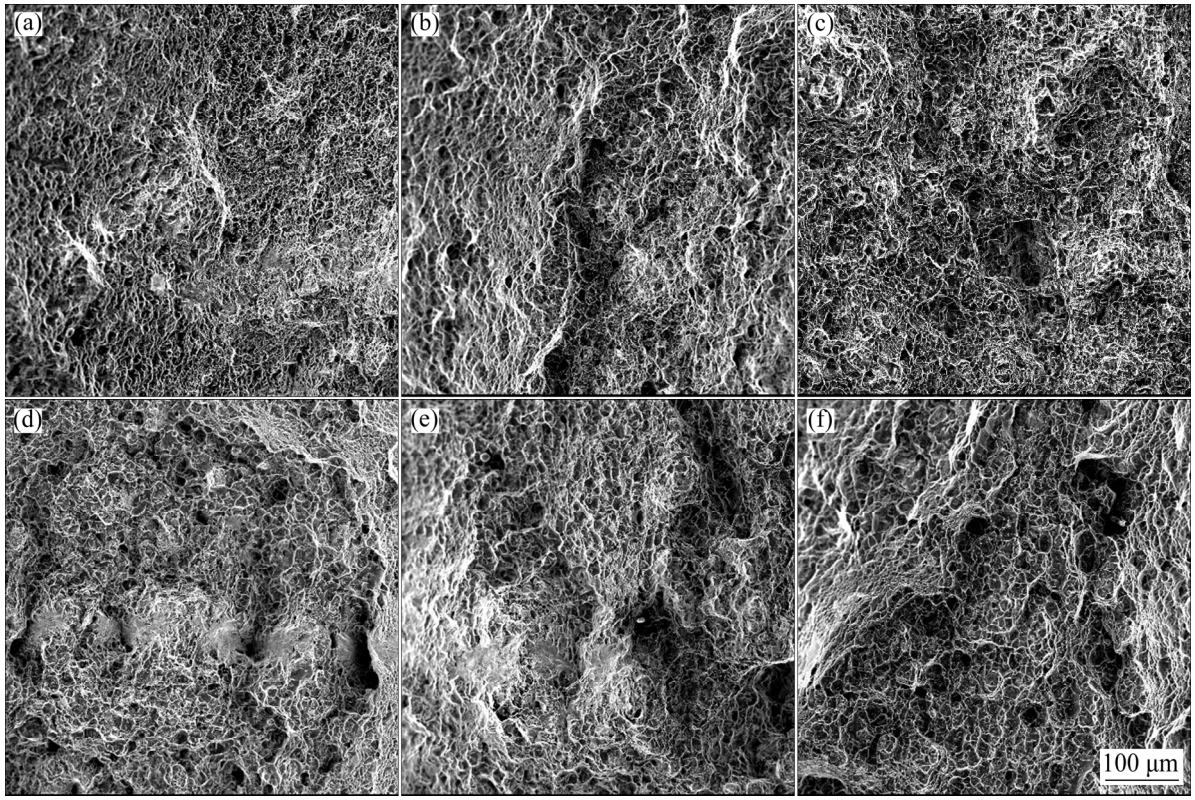

Fig. 11 Fracture surface morphologies of tensile specimens after annealing for different time: (a) As-received; (b) 2 h; (c) 3 h; (d) 5 h; (e) 6 h; (f) 8 h

microstructure features (including the size, volume fraction as well as the morphology of equiaxed α) become stable. Figure 11 shows the fracture surface morphologies of the tensile specimens after annealing for different time. The fracture surfaces become more rugged and the dimples distributed on them become much deeper and bigger with increasing annealing time, indicating improved plasticity. The information reflected from the fracture surface morphologies is consistent with the tensile results described above.

4 Conclusions

(1) The average α grain size shows a parabolic growth trend with increasing annealing time. Taking the annealing time of 5 h as demarcation point, the morphology of equiaxed α grains shows two changing stages. When the annealing time is below 5 h, the morphology of α grains changes from a short rod-like shape at the initial state to a near-spherical shape with increasing annealing time. However, when the annealing time is longer than 5 h, the morphology of equiaxed α grains changes towards polygonization.

(2) The activation energy for α boundary migration equals 138 kJ/mol, which is close to the activation energy for grain growth of pure α-Ti. This indicates that coarsening of equiaxed α is mainly due to self-diffusion of Ti atoms. Based on these findings, a static coarsening kinetics model of equiaxed α grains in the α+β field is established.

(3) The strength of the Ti811 alloy exhibits small fluctuations (30−40 MPa) and becomes stable after annealing for 3 h or longer. In contrast, the static coarsening behavior of equiaxed α shows a distinct influence on the plasticity. Due to the continuous coarsening of equiaxed α grains and polygonization of α grain boundaries, the elongation of the Ti811 alloy generally shows a two-step increase with increasing annealing time.

Acknowledgments

The authors are grateful for the financial supports from the China Scholarship Council (No. 201906935013) and the National Natural Science Foundation of China (No. 51801132).

References

[1] CUI C X, HU B M, ZHAO L C, LIU S J. Titanium alloy production technology, market prospects and industry development [J]. Materials & Design, 2011, 32(3): 1684−1691.

[2] SHI Z F, GUO H Z, ZHANG J W, YIN J N. Microstructure−fracture toughness relationships and toughening mechanism of TC21 titanium alloy with lamellar microstructure [J]. Transactions of Nonferrous Metals Society of China, 2018, 28(12): 2440−2448.

[3] LEYENS C, PETERS M. Titanium and titanium alloys [M]. Weinheim: WILEY-VCH Verlag GmbH & Co. KGaA, 2003.

[4] ZHAO H J, WANG B Y, JU D Y, CHEN G J. Hot tensile deformation behavior and globularization mechanism of bimodal microstructured Ti−6Al−2Zr−1Mo−1V alloy [J]. Transactions of Nonferrous Metals Society of China, 2018, 28(12): 2449−2459.

[5] LUO J, WANG B Z, WANG L F, LI L, LI M Q. Sensitivity analysis on globularized fraction of α lamellae in titanium alloys [J]. Transactions of Nonferrous Metals Society of China, 2019, 29(2): 305−312.

[6] SUN Z C, WANG X Q, ZHANG J, YANG H. Prediction and control of equiaxed α in near-β forging of TA15 Ti-alloy based on BP neural network: For purpose of tri-modal microstructure [J]. Materials Science and Engineering A, 2014, 591: 18−25.

[7] ZHEREBTSOV S, MURZINOVA M, SALISHCHEV G, SEMIATIN S L. Spheroidization of the lamellar microstructure in Ti−6Al−4V alloy during warm deformation and annealing [J]. Acta Materialia, 2011, 59(10): 4138−4150.

[8] BALDAN A. Review progress in Ostwald ripening theories and their applications to nickel-base superalloys. Part I: Ostwald ripening theories [J]. Journal of Materials Science, 2002, 37: 2171−2202.

[9] ARDELL A. The effect of volume fraction on particle coarsening: Theoretical considerations [J]. Acta Metallurgica, 1972, 20(1): 61−71.

[10] SEMIATIN S L, SUN F, CRIST E M, YU K O, SARGENT G A, SANDERS D G. Coarsening behavior and plastic flow of Ti−6Al−2Sn−4Zr−2Mo−0.1Si with an ultrafine microstructure [J]. Metallurgical and Materials Transactions A, 2016, 47: 4374−4377.

[11] SEMIATIN S L, KIRBY B C, SALISHCHEV G A. Coarsening behavior of an alpha-beta titanium alloy [J]. Metallurgical and Materials Transactions A, 2004, 35: 2809−2819.

[12] SARGENT G A, ZANE A P, FAGIN P N, GHOSH A K, SEMIATIN S L. Low-temperature coarsening and plastic flow behavior of an alpha/beta titanium billet material with an ultrafine microstructure [J]. Metallurgical and Materials Transactions A, 2008, 39: 2949−2964.

[13] MARTIN J W, DOHERTY R D, CANTOR B. Cambridge solid state science series: Stability of microstructure in metallic systems [M]. 2nd ed. Cambridge: Cambridge University Press, 1997.

[14] ATAPOUR M, PILCHAK A L, SHAMANIAN M, FATHI M H. Corrosion behavior of Ti−8Al−1Mo−1V alloy compared to Ti−6Al−4V [J]. Materials & Design, 2011, 32(3): 1692−1696.

[15] STROEVEN P, HU J. Review paper–stereology: Historical perspective and applicability to concrete technology [J]. Materials and Structures, 2006, 39: 127−135.

[16] WU C, YANG H, LI H W, YANG G B. Primary alpha grain coarsening behavior of Ti−6Al−2Zr−1Mo−1V alloy in the alpha+beta two-phase field [J]. Journal of Materials Engineering and Performance, 2013, 22: 2557−2566.

[17] UPMANYU M, SMITH RW, SROLOVITZ D J. Atomistic simulation of curvature driven grain boundary migration [J]. Interface Science, 1998, 6: 41−58.

[18] MASON J K. Grain boundary energy and curvature in Monte Carlo and cellular automata simulations of grain boundary motion [J]. Acta Materialia, 2015, 94: 162−171.

[19] PATTERSON B R, LIU Y. Relationship between grain boundary curvature and grain size [J]. Metallurgical Transactions A, 1992, 23: 2481−2482.

[20] GIL F J, PLANELL J A. Behaviour of normal grain growth kinetics in single phase titanium and titanium alloys [J]. Materials Science and Engineering A, 2000, 283(1−2): 17−24.

[21] SONG X Y, ZHANG J X, LI L M, YANG K Y, LIU G Q. Correlation of thermodynamics and grain growth kinetics in nanocrystalline metals [J]. Acta Materialia, 2006, 54(20): 5541−5550.

[22] JOHNSON C H, RICHTER S K, HAMILTON C H, HOYT J J. Static grain growth in a microduplex Ti−6Al−4V alloy [J]. Acta Materialia, 1998, 47(1): 23−29.

[23] GREWAL G, ANKEM S. Isothermal particle growth in two-phase titanium alloys [J]. Metallurgical Transactions A, 1989, 20: 39−54.

[24] ZHANG S S, LI M Q, LIU Y G, LUO J, LIU T Q. The growth behavior of austenite grain in the heating process of 300M steel [J]. Materials Science and Engineering A, 2011, 528(15): 4967−4972.

[25] LI W, XIA K. Kinetics of the α grain growth in a binary Ti−44Al alloy and a ternary Ti−44Al−0.15Gd alloy [J]. Materials Science and Engineering A, 2002, 329−331: 430−434.

[26] WANG T, GUO H Z, TAN L J, YAO Z K, ZHAO Y, LIU P H. Beta grain growth behaviour of TG6 and Ti17 titanium alloys [J]. Materials Science and Engineering A, 2011, 528(21): 6375−6380.

[27] MISHRA S, DEBROY T. Non-isothermal grain growth in metals and alloys [J]. Materials Science and Technology, 2006, 22(3): 253−278.

[28] FELTHAM P. Grain growth in metals [J]. Acta Metallurgica, 1957, 5(2): 97−105.

[29] STEINER R. History and progress on accurate measurements of the Planck constant [J]. Reports on Progress in Physics, 2013, 76(1): 1−46.

[30] SUN B, MENG XL, GAO Z Y, CAI W. Martensite structure and mechanical property of Ti−Nb−Ag shape memory alloys for biomedical applications [J]. Vacuum, 2018, 156: 181−186.

[31] WOOD R M. The lattice constants of high purity alpha titanium [J]. Proceedings of the Physical Society, 1962, 80(3):

783−786.

[32] ROTH T A, SUPPAYAKP. The surface and grain boundary free energies of pure titanium and the titanium alloy Ti−6Al−4V [J]. Materials Science and Engineering, 1978, 35(2): 187−196.

[33] XU W W, SHANG S L, ZHOU B C, WANG Y, CHEN L J, WANG C P, LIU X J, LIU Z K. A first-principles study of diffusion coefficients of alloying elements in dilute α-Ti alloys [J]. Physical Chemistry Chemical Physics, 2016, 18(25): 16870−16881.

Ti−8Al−1Mo−1V 合金等轴 α 相的静态粗化行为

石晓辉[1,2]，曹祖涵[1]，范智渊[1]，Jürgen ECKERT[2,3]，乔珺威[1]

1. 太原理工大学 材料科学与工程学院，太原 030024；

2. Erich Schmid Institute of Materials Science, Austrian Academy of Sciences, LeobenA-8700, Austria;

3. Department of Materials Science, Chair of Materials Physics, Montanuniversität Leoben, LeobenA-8700, Austria

摘　要：为深入了解 Ti−8Al−1Mo−1V 钛合金等轴 α 相在退火过程中的演变行为，基于粗化指数 n 及 α 界面迁移激活能的计算对其静态粗化机制进行研究。n=6 的结果表明，等轴 α 相具有特殊的粗化机制。计算得到的 α 界面迁移激活能为 138 kJ/mol，接近纯钛的晶粒长大激活能。这表明等轴 α 的粗化主要是由钛原子穿越 α/α 界面的自扩散导致。基于研究结果，建立等轴 α 相在 $\alpha+\beta$ 相区的静态粗化动力学模型。最后，分析等轴 α 相粗化行为对拉伸性能的影响。

关键词：静态粗化；动力学；模型；拉伸性能；Ti−8Al−1Mo−1V

(Edited by Bing YANG)